

# Halo Lum inosity Function From Photometric Calibration of the Revised NLTT

Andrew Gould, Juna A. Kolm eier, Julio Chanam e

Department of Astronomy, The Ohio State University, 140 W . 18th Ave., Columbus, OH  
43210

gould, jak, jchaname@astronomy.ohio-state.edu

Sam ir Salim

Department of Physics and Astronomy, University of California at Los Angeles, Los  
Angeles, CA 90095

samir@astro.ucla.edu

## ABSTRACT

We calibrate the photographic photometry of the revised New Luyten Two-Tenths catalog (rNLTT) by matching 3448 rNLTT stars to the Sloan Digital Sky Survey (SDSS). The correction is linear in magnitude and goes from zero at  $V = 14$  to 0.32 mag at  $V = 19$ , in the sense that rNLTT was previously too bright. The correction implies that the underlying USNO-A2.0 photometry, on which rNLTT photometry is based, is non-linear. The new calibration somewhat improves the appearance of the  $(V; V - J)$  reduced proper motion diagram in the sense of better separation between disk and halo stars. We repeat Gould's analysis of 5000 halo stars in rNLTT. The most important change is to move the peak of the halo luminosity function about 0.5 mag dimmer, from  $M_V = 10.5$  to  $M_V = 11$ , putting it into good agreement with the parallax-based determination of Dahn et al.

Subject headings: astrometry { catalogs { stars: fundamental parameters { stars: subdwarfs { late-type { white dwarfs

## 1. Introduction

The revised NLTT (rNLTT), assembled by Gould & Salim (2003) and Salim & Gould (2003), presented improved astrometry and photometry for approximately 36,000 stars drawn

from the New Luyten Two Tenths catalog (NLTT) (Luyten 1979, 1980). At the bright end, NLTT stars were matched primarily to the Hipparcos (ESA 1997) and Tycho-2 (Høg et al. 2000) catalogs, while at the faint end they were matched to USNO-A (Monet 1998) and 2MASS (Skrutskie et al. 1997). The bright end covers the whole sky. The faint end basically covers the 44% of the sky represented by the intersection of the 2MASS Second Incremental Release and First Palomar Observatory Sky Survey (POSS I), as reduced and cataloged by USNO-A. The roughly 45 year baseline between these observations enabled a proper motion precision of  $5.5 \text{ m as yr}^{-1}$ , roughly a 4-fold improvement over NLTT. By identifying USNO-A and 2MASS counterparts, rNLTT assigned  $(V;J)$  magnitudes to almost all entries, with  $V$  being derived from USNO-A photographic photometry in  $B_{\text{USNO}}$  and  $R_{\text{USNO}}$  and with  $J$  coming directly from 2MASS. This was a huge improvement over the original  $(B_{\text{NLTT}};R_{\text{NLTT}})$  photographic photometry of NLTT, in part because USNO-A photographic photometry has smaller scatter than Luyten's, but primarily because  $V - J$  provides a much longer color baseline than does  $B_{\text{NLTT}} - R_{\text{NLTT}}$ . Indeed, using a  $(V;V - J)$  reduced proper motion (RPM) diagram, Salim & Gould (2002) were able for the first time to cleanly separate main-sequence, subdwarf, and white dwarf stars in NLTT. This clean separation then permitted Gould (2003a) to analyze a sample of 4500 halo stars and to measure their luminosity function and velocity distribution with much greater precision than was previously possible. The improved astrometry and photometry of rNLTT also permitted Chanamé & Gould (2004) to assemble a catalog with more than 1000 wide binaries, also cleanly separated into disk and halo objects.

The photometric calibration of the rNLTT optical ( $V$ ) band was derived by comparing USNO-A photometry of NLTT stars with photometry found in the literature for the same stars, including 36 white dwarfs from Liebert et al. (1988) and 19 M dwarfs from Weis (1996). While the sample covered a broad range of magnitudes,  $11 < V < 18$ , the small sample size led Salim & Gould (2003) to solve only for a zero point and a color term but to assume that the flux levels derived from USNO-A magnitudes were linear in flux. A proper calibration would require a sample that is both large and covers the full range  $12 < V < 19$  from the magnitude limit of Tycho-2 (and hence the onset of USNO-A-based photometry) to the magnitude limit of rNLTT.

The Sloan Digital Sky Survey (SDSS) Data Release 3<sup>1</sup> (Abazajian et al. 2005) now provides such a sample and so permits a calibration of rNLTT photometry over the entire range  $12 < V < 19$ . We carry out this calibration and find that rNLTT assigned  $V$  magnitudes that are too bright by an amount that grows linearly with increasing  $V$ . That is,

---

<sup>1</sup><http://www.sdss.org/dr3>

$V = 0.0633(V - 13.9)$ . Because this offset is of order the statistical photometric error of 0.22 mag, it is too small to have any practical impact on applications that use rNLTT to locate interesting classes of stars, such as subdwarfs (Yong & Lambert 2003), white dwarfs (Vennes & Kawka 2003; Kawka et al. 2004), red dwarfs (Reid et al. 2004), and dwarf carbon stars (Lowrance et al. 2003). However, because the effect is systematic, it could potentially affect studies that derive parameters from a statistical analysis of rNLTT. In this case, the fractional errors in the derived parameters can be much smaller than the errors associated with individual stars.

In some respects, rNLTT has already been superseded by the Lepine & Shara (2005) proper motion catalog (LSPM), which covers the entire northern sky,  $V < 19$ . LSPM has a proper motion threshold of  $150 \text{ m asyr}^{-1}$  (compared to  $180 \text{ m asyr}^{-1}$  for NLTT) and is more complete than NLTT (and indeed is virtually 100% complete to  $V = 19$ ). *Ipsa facto*, LSPM is more complete than rNLTT in the region it covers. However, rNLTT has significantly smaller astrometric errors ( $5.5$  vs.  $8 \text{ m asyr}^{-1}$ ) and somewhat smaller photometric errors and also covers areas south of the equator. While all three of these shortcomings can be rectified in principle, substantial additional work will be required. Moreover, the photometry and astrometry improvements would be achieved by cross-identifying LSPM stars with USNO-A, and when this is done, the photometric calibration presented here will still have to be applied.

Finally, Gould (2003a)'s statistical analysis of rNLTT halo stars will form a baseline of comparison for future studies based on even larger proper motion samples. It is therefore important to remove systematic effects in this analysis.

## 2. Calibration

Our basic plan of attack is to cross identify rNLTT with SDSS (third data release) in order to plot  $V - V_{\text{SDSS}} - V_{\text{rNLTT}}$ , where

$$V_{\text{SDSS}} = r + 0.44(g - r) - 0.02 \quad (1)$$

is the transformation of SDSS magnitudes into Johnson  $V$  as calibrated by Juric et al. (2002) and

$$V_{\text{rNLTT}} = R_{\text{USNO}} + 0.32(B - R)_{\text{USNO}} + 0.23 \quad (2)$$

is the transformation from USNO-A2 magnitudes into Johnson  $V$  as used in rNLTT. Juric et al. (2002) estimate that the SDSS calibration reproduces Johnson  $V$  to "better than 0.05 mag". Before proceeding, we note that equation (2) applies directly only for stars  $V > 20$ , where rNLTT derives its photometry and astrometry from USNO-A2.0. For

33 . . . 20 , rNLT T uses USNO -A 1.0, which requires a photometric conversion given by Salim & Gould (2003) before applying equation (2). However, since all SDSS areas lie in the former region, this photometric conversion plays no role in the current work.

In order to assure a clean sample, we restrict the selection as follows. First, we consider only SDSS stars with proper motion entries, derived from USNO -B1.0 (Monet et al. 2003) cross identifications,  $\mu > 140 \text{ m asyr}^{-1}$ . Second, we exclude SDSS stars with a "bad" position on the gri color-color diagram. Here "bad" means away from the characteristic "dog-leg" stellar locus of this diagram, except that we allow stars with degenerate M-dwarf g-r colors ( $1.2 < g-r < 1.8$ ) but with anomalously low flux due to saturation. Third, we consider only rNLT T stars that are matched to both USNO -A and 2MASS and with  $V_{\text{rNLT T}} > 12$ . Fourth, we exclude rNLT T stars with binary companions within  $10^0$ . Fifth, we demand that the rNLT T epoch 2000 position agree with the SDSS position to within  $3^0$ . Finally, we exclude matches with discrepant proper motions (vector difference greater than  $30 \text{ m asyr}^{-1}$ ), unless their positions lie within  $1^0$ .

SDSS (by virtue of USNO -B) and rNLT T (based on USNO -A) both use POSS I for the first epoch of their proper motion estimates, so the first condition implies a high probability that if there is a position match, it is to a genuine rNLT T star. SDSS photometry can be compromised by saturation, and this is particularly a worry for stars at the bright end of our investigation. The gri test should exclude most saturated stars. However, if the g-r color is consistent with the degenerate M-dwarf track, we do not want to exclude the star simply because the measurement is corrupted. This is to be expected for bright, red stars, but does not interfere with our V-band estimate (which depends only on g and r). The third condition is motivated by the fact that while rNLT T does contain entries that are missing either USNO -A or 2MASS data, these identifications are generally less secure. Moreover, in the former case, of course, its V estimate is not based on USNO -A photometry. The fourth condition is imposed because USNO -A photometry can be corrupted by the presence of a near neighbor. In general, we allow for a  $3^0$  mismatch in position because SDSS positions are given at the epoch of observation while rNLT T positions are at epoch 2000. For high proper motion stars there can be a significant offset. However, we guard against random matches by demanding  $1^0$  agreement unless the proper motions differ by less than  $30 \text{ m asyr}^{-1}$ .

In Figure 1, we plot  $V_{\text{SDSS}} - V_{\text{rNLT T}}$  for the sample of 3448 matches obtained in this way. We fit these points to a straight line and estimate the error from the scatter by demanding that  $\chi^2$  per degree of freedom (dof) be equal to unity. We eliminate the largest outlier and repeat this procedure until the largest outlier is less than  $3\sigma$ . This results in 51 eliminations compared to 10 that would be expected from a strictly Gaussian distribution. That is,

non-Gaussian outliers constitute 1% of the sample. We find,

$$V_{SDSS} - V_{NLTT} = (0.1331 - 0.0039) + (0.0633 - 0.0024)(V_{NLTT} - 16); \quad (3)$$

with a scatter of  $\sigma = 0.22$  mag, where the zero-point offset ( $V_{NLTT} - 16$ ) is chosen to minimize (among integer values) the correlation between the two terms. This relation implies that relatively faint stars ( $V > 14$ ) should be corrected to still fainter  $V$  magnitudes, and hence also redder  $V - J$  colors. Because the slopes of main sequence and subdwarf sequence are greater than unity, the color change has a bigger impact, so that both of these sequences become brighter at fixed color.

We try extending this linear fit to next order, but find that the additional quadratic term does not significantly improve the fit. Similarly, we find no correlation between the residuals to the fit and observed  $V - J$  color.

Equation (3) implies that USNO-A2.0 photometry is non-linear. By combining this equation with equation (2), we derive an explicit expression for this nonlinearity,

$$V_{SDSS} = 1.0633R_{USNO} + 0.3403(B - R)_{USNO} - 0.6351 \quad (4)$$

While SDSS photometry is quite homogeneous, this is not necessarily true of USNO-A photometry, which is derived from photographic plates exposed under strongly varying conditions. Our principal concern is not plate-to-plate variations, which would be too localized to affect most statistical applications, but possible broad trends with position on the sky. We therefore divide the data into seven different subsets, the four quadrants in right ascension and three bands in declination (separated at  $\delta = 0$  and  $\delta = 40$ ). The only significant differences that we find are for the ( $\alpha < 0$ ) and ( $0 < \alpha < 40$ ) subsamples, which have zero points that are respectively about 0.035 mag greater and 0.025 mag smaller than the sample as a whole. While these deviations are detected with high (almost 7 $\sigma$ ) confidence, they are quite small compared to the scatter of 0.22 mag. We will ignore them in what follows, but for some applications the reader should be aware that they are present.

Figure 2 shows the  $mNLTT$  ( $V; V - J$ ) RPM diagram before and after correcting the photometry. What is plotted is not the traditional RPM but the parameter

$$V_{rpm,adj} = V + 5 \log \left( \frac{1.47j \sin b_j}{2.73} \right); \quad (5)$$

where  $\mu$  is the proper motion in arcsec per year and  $b$  is the Galactic latitude. As shown by Salim & Gould (2003), adding the Galactic-latitude term yields a cleaner separation of disk and halo stars. The line,  $\mu = 0$ , where

$$V_{rpm,adj} = 3.1(V - J) \quad (6)$$

is the boundary separating these populations that was adopted by Salim & Gould (2003). The principal change is that stars in the lower portions of the diagram are shifted to the red because the  $V$  measurements are now fainter. (Of course, they are also shifted down, but this is less noticeable.) In addition, the "trough" between the disk and halo tracks now appears both straighter and somewhat cleaner. The  $\beta = 0$  line still appears to be a good boundary to separate stars that are most likely in the halo from those in the disk or thick disk. However, the boundary for secure halo stars can be placed at  $\beta = 0.5$ , rather than at  $\beta = 1.0$ , as was adopted by Gould (2003a).

### 3. Halo Parameters

We fit the halo stars in mNLTT (with the newly recalibrated photometry) to the 28-parameter halo model of Gould (2003a). We apply almost exactly the same procedures as in the original work, which we review very briefly here.

#### 3.1. Review of Model and Method

The model contains 13 parameters to describe the luminosity function (LF),  $(M_{V,i}); i=3:::15$ , one for each 1-magnitude bin from  $M_V = 3$  to  $M_V = 15$ . It has 9 parameters describing the halo velocity ellipsoid including 3 for bulk motion relative to the Sun ( $U_i$ ) and 6 for the velocity dispersion tensor [ $\beta$  dispersions  $c_{ii}$  and 3 correlation coefficients,  $c_{ij} = (C_{ii}C_{jj})^{1/2}$ ]. The halo color-magnitude relation (CMR) is described by 2 parameters ( $a;b$ ), i.e.,  $M_V = a(V - J)_0 + b$ . There are 2 parameters describing the halo density profile ( $\gamma; z_0$ ), i.e.,  $\rho = \rho_0 (R/R_0)^{-\gamma} \exp(-z/z_0)$ . Here,  $R$  is Galactocentric distance,  $R_0 = R(\text{sun})$ ,  $z$  is distance from the plane,  $\gamma$  is the halo density power law, and  $z_0$  is the inverse scale height. Finally, there are 2 parameters describing the sample completeness,  $V_{\text{break}}$  and  $f_{\text{break}}$ . The sample is assumed 100% complete for  $V < 12$  and then to fall linearly to  $f_{\text{break}}$  at  $V_{\text{break}}$ , and then to fall linearly from there to zero at  $V = 20$ . Of these 28 parameters, one is held fixed at  $U_2 = 216.6 \text{ km s}^{-1}$  in order to enforce an otherwise unconstrained distance scale.

The best-fit model is found by maximizing the likelihood

$$\ln L = \sum_{k=1}^{N_{\text{det}}} \ln f P_k [z^m(z_{\text{obs}}^m)] / N_{\text{exp}} \quad (7)$$

where  $N_{\text{det}}$  is the number of stars in the sample,  $N_{\text{exp}}$  is the number expected in the model,  $z^m$  are the  $m = 6$  phase space coordinates per star in the model,  $z_{\text{obs}}^m$  are the  $m = 6$  observables

$(l; b; l_1; b_1; V; J)$  from which these coordinates are inferred,  $P_k$  is the probability that the  $k$  star will have the phase-space coordinates that have been inferred from the observations given the model parameters, and  $J$  is the Jacobian of the transformation from the observables to the phase-space coordinates. (Note that the rows in the second matrix of Gould 2003a's eq. [6] should be reversed, but that the final result is correct.) The number expected ( $N_{\text{exp}}$ ) in each trial model is evaluated by Monte Carlo integration, which is populated at 100 times higher density than the actual sample to suppress Poisson errors. However, to avoid fluctuations when comparing one model to another, the random positions and velocities are chosen only once, and then are assigned different weights depending on the model parameters.

Gould (2004) found a bug in the likelihood code used by Gould (2003a) and gave revised parameters corrected for this bug. However, most of the corrections were very small.

### 3.2. Changes in Approach

We implement two major changes relative to Gould (2003a)'s treatment (in addition to using the recalibrated photometry). First, based on inspection of Figure 2, we select stars in the interval  $0.5 < \text{parallax} < 15$ . This yields a sample of 5042 "secure halo stars", somewhat larger than the 4588 analyzed by Gould (2003a) (and corrected to 4564 in Gould 2004).

Second, we discovered that Gould (2003a)'s likelihood maximization routine was too "stiff" to probe the effect of simultaneous changes in the two color-magnitude parameters,  $(a; b)$ , and the LF,  $(M_{v,i})$ . When either or both of the color-magnitude parameters change, this affects all of the LF parameters. Unless all can be varied simultaneously in just the right way, the true maximum cannot be located. We address this problem using the method of "hybrid statistical errors" of An et al. (2002). We hold the two color-magnitude parameters  $A_i^{(a,b)} = (a; b)$  fixed at a grid of values and evaluate the likelihood  $L$  for the remaining 25 free parameters  $A_k^{(\text{remain})}$ . We then find the inverse covariance matrix for the color magnitude parameters,

$$B_{ij}^{(a,b)} = \frac{\partial^2 L}{\partial A_i^{(a,b)} \partial A_j^{(a,b)}} \quad (8)$$

and so obtain the restricted covariance matrix  $C^{(a,b)} = [B^{(a,b)}]^{-1}$ . We also find the gradient of all 27 parameters with respect to the two color-magnitude parameters over the grid of solutions,  $\partial A_k = \partial A_i^{(a,b)}$ . We determine the covariance matrix,  $C_{ij}^{(\text{remain})}$  of the remaining 25 free parameters (with  $[a; b]$  held fixed at their likelihood maximum) using the bootstrap

technique. Finally, we find the hybrid covariance matrix

$$C_{ij} = C_{ij}^{(\text{remain})} + \sum_{m,n} C_{m,n}^{(a;b)} \frac{\partial A_i}{\partial A_m^{(a;b)}} \frac{\partial A_j}{\partial A_n^{(a;b)}} : \quad (9)$$

### 3.3. Results

As discussed below equation (3), the primary changes in the data set are to make the faint stars fainter absolutely, but to make the tracks of subdwarf (and main-sequence) stars brighter at fixed color. Hence, we expect that the main changes in the fit will be to make the CMDR fainter and shallower, and to move the peak in the LF toward fainter magnitudes. Table 1 shows that these are indeed the main effects. The first two columns give the parameter name and units. The next two give the best fit values as determined using the old and new photometric calibration, respectively. The final two columns give the respective errors.

Figure 3 shows the new LF together with several other determinations from the literature. Comparing this figure to Figure 2 from Gould (2004) (of which it is an updated version), one sees that the rNLTT-based LF has moved toward very good agreement with the LF of Dahn et al. (1995) (DLHG) as renormalized by Gould (2003a) using the results of Casertano et al. (1990) (CRB). Indeed, with the exception of the final DLHG/CRB point, the two are in agreement at the 1 level. This resolves an important puzzle: the two determinations are both essentially local and so should be similar. It would be quite surprising if their peaks were separated by a magnitude, as appeared to be the case before the rNLTT photometry was recalibrated.

There are a few other changes that should be noted as well. First, while most of the error bars are similar with the old and new photometry, those of the two color-magnitude parameters (a;b) and of the three velocity dispersions ( $c_{ii}$ ) have all grown significantly. As mentioned above, the previous algorithm was too stiff to properly evaluate the errors in (a;b), so it is not surprising that they have grown. This growth is also responsible for the increase in the  $c_{ii}$  errors through the second term in equation (9), which was not previously incorporated. Of course, this term also increases the errors of all other parameters, but it turns out that these other increases are mostly not significant relative to the errors given by the first term.

Another significant change is that the break in the completeness function,  $V_{\text{break}}$  has moved about 1/2 mag fainter. This is also not surprising given that the whole photometric calibration has moved fainter at the faint end. However, the completeness level at this break has also moved lower, and this has disturbing consequences, as we discuss in the next section.



Finally, we note that the two bulk velocity parameters and three velocity-ellipsoid correlation coefficients  $(U_1; U_3; e_{12}; e_{13}; e_{23}) = (10.6 \pm 1.4; 6.4 \pm 1.8; 0.017 \pm 0.015; 0.010 \pm 0.017; 0.036 \pm 0.025)$  remain very close to the values expected in an axisymmetric Galaxy,  $(10.0; 7.2; 0; 0; 0)$ , when account has been taken of the Sun's motion with respect to the local standard of rest  $(10.00 \pm 0.36; +7.17 \pm 0.38) \text{ km s}^{-1}$  in the radially outward and vertical directions (Dehnen & Binney 1998). This yields a  $\chi^2 = 4.04$  for 5 degrees of freedom, almost identical to the value 3.97 obtained by Gould (2003b) from the halo solution of Gould (2003a). This implies that the constraints on the granularity of the stellar halo derived by Gould (2003b) from this  $\chi^2$  determination remain unaltered.

#### 4. Two Puzzles

While it is comforting to see the old puzzle regarding the peak of the halo LF resolved (see §3.3), the halo solution derived using recalibrated rNLT T photometry presents two new puzzles. These concern conflicts with independent determinations of NLT T completeness and of the  $(V; V_{\text{J}})$  CMR.

##### 4.1. Completeness

The completeness fraction ( $f_{\text{break}} = 0.38$ ) at the completeness break point ( $V_{\text{break}} = 18.8$ ) seems quite low. Gould (2003a) had argued that a somewhat higher value was consistent with what was then otherwise known about the completeness of NLT T (see also Gould 2004). However, not only is the new value of  $f_{\text{break}}$  lower, but Lepine & Shara (2005) have shown, using their own independent and very complete northern-sky proper-motion catalog, that at high latitude,  $b > 15^\circ$ , NLT T is 85% complete at  $V = 18.5$ . We now explore several ideas to resolve this conflict, but the executive summary is: none are successful.

First, the Lepine & Shara (2005) completeness estimate strictly applies only for proper motions  $> 250 \text{ m asyr}^{-1}$ , whereas rNLT T goes down to  $180 \text{ m asyr}^{-1}$ . Completeness falls to 79% at  $V = 18.5$  for  $> 200 \text{ m asyr}^{-1}$ . However, this "incompleteness" is simply due to NLT T's  $20 \text{ m asyr}^{-1}$  errors combined with its  $180 \text{ m asyr}^{-1}$  threshold: stars that are mis-measured below this threshold due to normal statistical errors are not included in the catalog. This effect is already taken into account in our likelihood procedure. Moreover, even if it were not accounted for, the effect is much smaller than the discrepancy and so could not account for it in any case.

Second, rNLT T is less complete than NLT T, and the halo sample used here is less

complete than  $rNLT$ , primarily because stars without J-band data are excluded. However, as shown by Salim & Gould (2003),  $rNLT$  is about 97% complete relative to  $NLT$  down to  $R_{NLT} = 17$  and 95% complete at  $R_{NLT} = 18$ . These magnitudes correspond roughly to  $V = 17.5$  and  $V = 18.5$ , respectively. It is true that the completeness at the faint end is substantially worse if one excludes stars without J-band data. However, as was argued by Salim & Gould (2003) and strikingly confirmed by Lepine & Shara (2005), almost all faint  $NLT$  stars that lack 2MASS counterparts are white dwarfs, not subdwarfs. Hence, incompleteness of  $rNLT$  relative to  $NLT$  can explain at most a few percent of the effect.

Third, the form of the completeness function adopted by Gould (2003a), and summarized above in §3.1, could in principle be too simple to capture the evolution of  $NLT$  completeness over 8 magnitudes. In fact, however, from Figure 22 of Lepine & Shara (2005), this form actually looks quite appropriate, except that the parameters should rather be  $f_{break} = 0.8$ ,  $V_{break} = 18.7$ . Nevertheless, we further test this possibility by eliminating the faintest stars in the likelihood sample  $V > 18.5$ , and re-fitting with a simple 1-parameter completeness function,  $f_{break}$  at  $V = 18.5$ . We find a best-fit  $f_{break} = 0.39$ . If we enforce  $f_{break} = 0.80$  (to take account of both the 15%  $NLT$  incompleteness and the 5% incompleteness of  $rNLT$  relative to  $NLT$  at the faint end), then the likelihood falls by 25, which means that this potential solution is ruled out at the 7 $\sigma$  level. To be conservative, we repeat this exercise with the cutoff at  $V = 18$ , but still find that the best-fit  $f_{break} = 0.41$  is preferred at the 7 $\sigma$  level over the independently-determined value of  $f_{break} = 0.85$ .

Is it possible that Lepine & Shara (2005) overestimated the completeness of  $NLT$ ? We believe not. At high latitudes, they failed to detect only 1% of  $NLT$  stars. They tracked down the reason for this failure in each case and found in essentially all cases that the star was contaminated by a random field star in their own (circa 1990) second epoch, but was free from contamination in  $NLT$ 's (circa 1970) second epoch. They inferred that they were missing an additional 1% from stars corrupted in the common  $NLT/LSPM$  (circa 1950) first epoch. Hence,  $LSPM$  is itself nearly 100% complete and so forms an excellent template against which to measure the completeness of  $NLT$ .

If  $f_{break}$  is forced to high values, then most of the parameters in the halo fit remain unchanged. However, the LF is suppressed by an amount that decreases from a factor 1 at the bright end to a factor  $f_{break} = 0.8$  at the faint end. Such an adjustment would engender a conflict between the DLHG/CRB LF and the one derived from the halo fit. However, as we discuss in the next section, this in itself is not a strong argument against making the adjustment. The principal argument is simply that it leads to a poor fit to the  $rNLT$  data. In brief, at present we see no clear path to resolving this conflict.

## 4.2. Color-Magnitude Relation (CMR)

The second puzzle concerns the CMR. Gould (2003a) derived a CMR from stars with trigonometric parallaxes taken from Monet et al. (1992) and Gizis (1997) that was quite consistent with the CMR derived from the halo likelihood fit. Indeed, the two CMRs lie almost exactly on top of one another in his Figure 3. However, after photometric recalibration, our new CMR has changed, while the parallax-based CMR should remain essentially the same. In fact, we slightly change our selection of parallax stars to be consistent with our "secure halo" criterion,  $0.5 < \pi < 1.5$ , but the impact of this change is expected to be small.

Before restricting attention to the halo stars, we first find the mean photometric offset between the CCD  $V$  magnitudes given by Monet et al. (1992) and Gizis (1997) and the recalibrated rNLTT  $V$  magnitudes for the entire sample of 58 rNLTT-parallax stars with  $V > 12$ . We find a mean difference  $0.03 \pm 0.04$  mag, in the sense that recalibrated rNLTT is brighter. The fact that the two are consistent at the 1 $\sigma$  level serves as a sanity check on the SDSS-based calibration, although the smaller number of parallax stars makes the uncertainty in this test uncompetitive with SDSS.

As Gould (2003a) did, we eliminate the reddest star on the ground that the CMR for the latest-type stars may deviate from a straight line and take a turn toward the red. (There are too few very late subdwarfs in the rNLTT sample to test this conjecture, so it is better to just eliminate this star from the comparison.) We use the CCD photometry both to make the selection (i.e., determine  $\tau$ ), and to estimate the absolute magnitude. This yields a sample of 23 rNLTT-parallax halo stars. We find that we must add an error  $(\sigma_V) = 0.72$  in quadrature to the errors propagated from the given parallax errors, in order to achieve  $\chi^2_{\text{dof}} = 1$ . Fitting to the form  $M_V = a(V - J)_0 + b$ , we find,

$$a = 3.668 \pm 0.396; \quad b = 0.324 \pm 1.201; \quad r = 0.9906 \quad (\text{parallax CMR}) \quad (10)$$

compared to the values

$$a = 3.339 \pm 0.027; \quad b = 0.921 \pm 0.073; \quad r = 0.8948 \quad (\text{halo fit}) \quad (11)$$

obtained in the halo fit in §3.3. Here  $r$  is the correlation coefficient. Figure 4 shows the parallax data with various CMRs.

While the slopes and zero points of equations (10) and (11) are each consistent at the 1 $\sigma$  level, the two are highly correlated, so that the relations as a whole are mildly inconsistent, with  $\chi^2 = 4.0$ . To interpret this discrepancy, we must first ask how the slope and zero point of the halo-fit CMR depend on the data and the assumptions. The slope is determined fairly directly from the rNLTT data themselves and primarily reflects the slope of the "subdwarf

sequence" seen in the RPM diagram (Fig. 2). On the other hand, the zero point is directly determined by fixing  $U_2 = 216.6 \text{ km s}^{-1}$ . If this value had been fixed 10% faster, then all of the 5 other velocity parameters would have increased in lock step by the same 10%, and all the inferred distances would have increased by the same amount. This rigid scaling occurs because (apart from a very slight effect in the extinction prescription) the only way that the distance scale enters the likelihood calculation is through  $U_2$ . This distance scaling then implies that the LF would have been reduced uniformly by a factor  $(1.1)^3$ . However, the value of  $U_2 = 216.6 \text{ km s}^{-1}$  was adopted directly from the statistical parallax solution of Gould & Popowski (1998) and is therefore to some extent arbitrary. First, that measurement had a 1 $\sigma$  statistical error of  $12.5 \text{ km s}^{-1}$ . Second, as Gould & Popowski (1998) (and references therein) note, different selection criteria will yield halo samples with values of  $U_2$  that differ by of order  $10 \text{ km s}^{-1}$ . Gould (2003a) argued that the " $\chi^2$ " selection criterion used in his (and our) halo analysis was most similar to that of Gould & Popowski (1998), but there could still be some differences between the samples. Combining these two effects, the true value of  $U_2$  might plausibly be different from the adopted one by of order  $15 \text{ km s}^{-1}$ , corresponding to 0.15 mag in the CMR zero point.

Hence, when combining the two CMRs, we should insist on a common slope, but initially allow the two zero points to differ. Since the halo- $t$ 's slope error is about 15 times smaller than that of the parallax determination, this amounts to fixing the parallax-based slope at the halo- $t$  value. The parallax-based zero point then becomes  $b = 1.31 \pm 0.16$ , which is 0.29 mag fainter than the halo- $t$   $b = 0.92$ . The direction of this discrepancy may seem surprising at first sight because the photometric recalibration moved the halo stars toward fainter mags, yet the CMR based on these stars has now become brighter than the parallax-based CMR. The reason is that the halo stars became not only fainter but redder, and because the slope of the CMR is larger than unity, the latter is the larger effect. Hence, at fixed color (which is what is important for the CMR), the halo stars have become brighter, even though they are fainter absolutely.

Having reasoned through the problem heuristically and verified that the two CMRs give qualitatively similar results, we combine them in a formally rigorous way by averaging the two  $(a;b)$  vectors, each weighted by its inverse covariance matrix. To take account of the external error due to uncertainty in the Gould & Popowski (1998) velocity input, we first add 0.15 mag to the halo- $t$  uncertainty in  $b$ . We then find

$$a = 3.3438 \pm 0.0269 \quad b = 1.091 \pm 0.134; \quad \mu = 0.543 \quad (\text{combined determinations}) \quad (12)$$

At the " $\chi^2$  center of mass" of the halo-star color distribution,  $V - J = 2.4$ , this relation is  $0.17 \pm 0.10$  mag fainter than the CMR derived from the halo- $t$  alone (but assuming a known  $U_2$ ).

Hence, taking account of this calibration (and the added uncertainty in the  $U_2$  constraint) the velocities should all be smaller by a factor  $0.93 \pm 0.04$ , while the LF should be higher by a factor  $1.26 \pm 0.16$ . These changes are not large, but they do mean that one cannot demand too close agreement between the LF derived from the NLT sample and that derived from local star counts by DLHG/CRB (see x 4.1).

Work by AG and JAK was supported by grant AST 02-01266. Work by JC was supported by an Ohio State University Presidential Fellowship.

R E F E R E N C E S

- Abazajian, K . 2005, *AJ*, submitted (astro-ph/0410239)
- An, J.H ., et al. 2002, *ApJ*, 572, 521
- Bahcall, J.N ., & Casertano, S. 1986, *ApJ*, 308, 347
- Casertano, S., Ratnatunga, K ., & Bahcall, J.N . 1990, *ApJ*, 357, 435
- Chaname, J., & Gould, A . 2004, *ApJ*, 601, 289
- Dahn, C.C ., Liebert, J.W ., Harris, H ., & Guetter, H.C . 1995, p. 239, *An ESO Workshop on: the Bottom of the Main Sequence and Beyond*, C.G. Tinney ed. (Heidelberg: Springer)
- Dehnen, W . & Binney, J.J. 1998, *MNRAS*, 298, 387
- European Space Agency (ESA) . 1997, *The Hipparcos and Tycho Catalogues* (SP-1200; Noordwijk: ESA)
- Gizis, J.E . 1997, *AJ*, 113, 508
- Gould, A . 2003a *ApJ*, 583, 765
- Gould, A . 2003b, *ApJ*, 592
- Gould, A . 2004 *ApJ*, 607, 653
- Gould, A ., Flynn, C ., & Bahcall, J.N . 1997, *ApJ*, 503, 798
- Gould, A . & Popowski, P. (1998) *ApJ*, 508, 844
- Gould, A ., & Salm, S., 2003, *ApJ*, 582, 1001
- Høg, E . et al. 2000, *A&A*, 355, L27
- Juric, M . et al. 2002, *AJ*, 124, 1776
- Liebert, J., Dahn, C.C ., & Monet, D.G . 1988, *ApJ*, 332, 891
- Kawka, A ., Vennes, S., Thorstensen, J.R . 2004, *AJ*, 127, 1702
- Lepine, S. & Shara, M.M . 2005, *AJ*, in press (astro-ph/0412070)
- Lorraine, P.J., Kirkpatrick, J.D ., Reid, I.N ., Kelle, L.C ., & Liebert, J. 2003, *ApJ*, 584, L98

- Luyten, W .J. 1979, 1980, *New Luyten Catalogue of Stars with Proper Motions Larger than Two Tenths of an Arcsecond* (Minneapolis: University of Minnesota Press)
- Monet, D .G . 1998, *American Astronomical Society Meeting*, 193, 112003
- Monet, D .G ., Dahn, C .C ., Vrba, F .J., Harris, H .C ., Pier, J.R ., Luginbuhl, C .B ., & Ables, H .D . 1992, *AJ*, 103, 638
- Monet et al. 2003, *AJ*, 125, 984
- Reid, I.N . 2004, *AJ*, 128, 463
- Salim, S. & Gould, A ., 2002, *ApJ*, 575, L83
- Salim, S., & Gould, A . 2003 *ApJ*, 582, 1011
- Skrutskie, M .F . et al. 1997, in *The Impact of Large-Scale Near-IR Sky Survey*, ed. F .G arzon et al (Kluwer: Dordrecht), p. 187
- Vennes, S. & Kawka, A . 2003, *ApJ*, 586, L95
- Weis, E .W . 1996, *AJ*, 112, 2300
- Yong, D . & Lambert, D .L . 2003, *AJ*, 126 2449

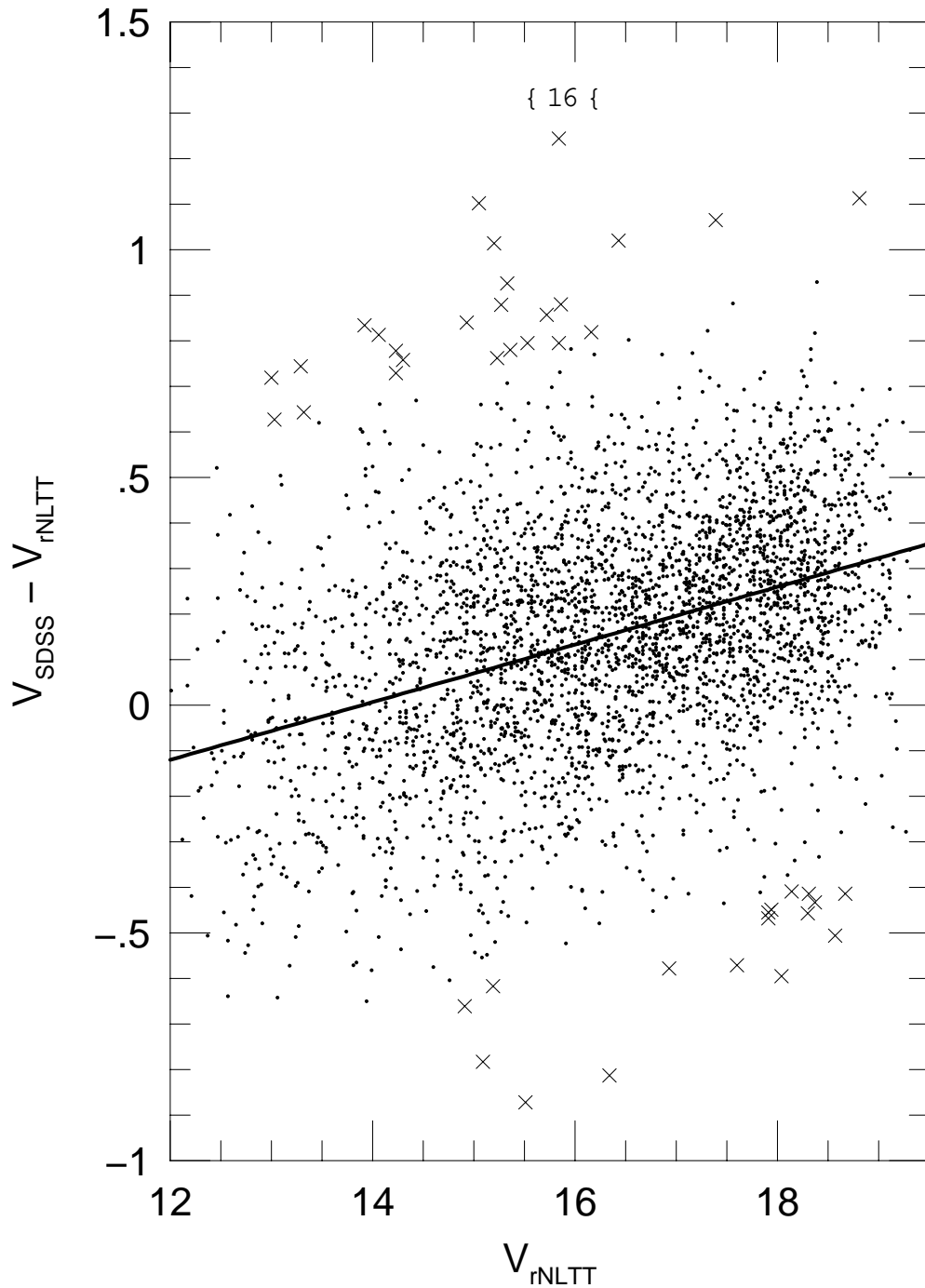


Fig. 1. | Difference ( $V = V_{\text{SDSS}} - V_{\text{rNLTT}}$ ) between V band measurements as derived from SDSS CCD photometry and rNLTT (ultimately USNO-A) photographic photometry for 3448 stars in common. Crosses indicate the 51 recursively removed 3 outliers. The remaining points are fit to a straight line  $V = 0.1331 + 0.0633(V_{\text{rNLTT}} - 16)$ , which is shown in bold. The residual scatter of these 3397 points is 0.22 mag.



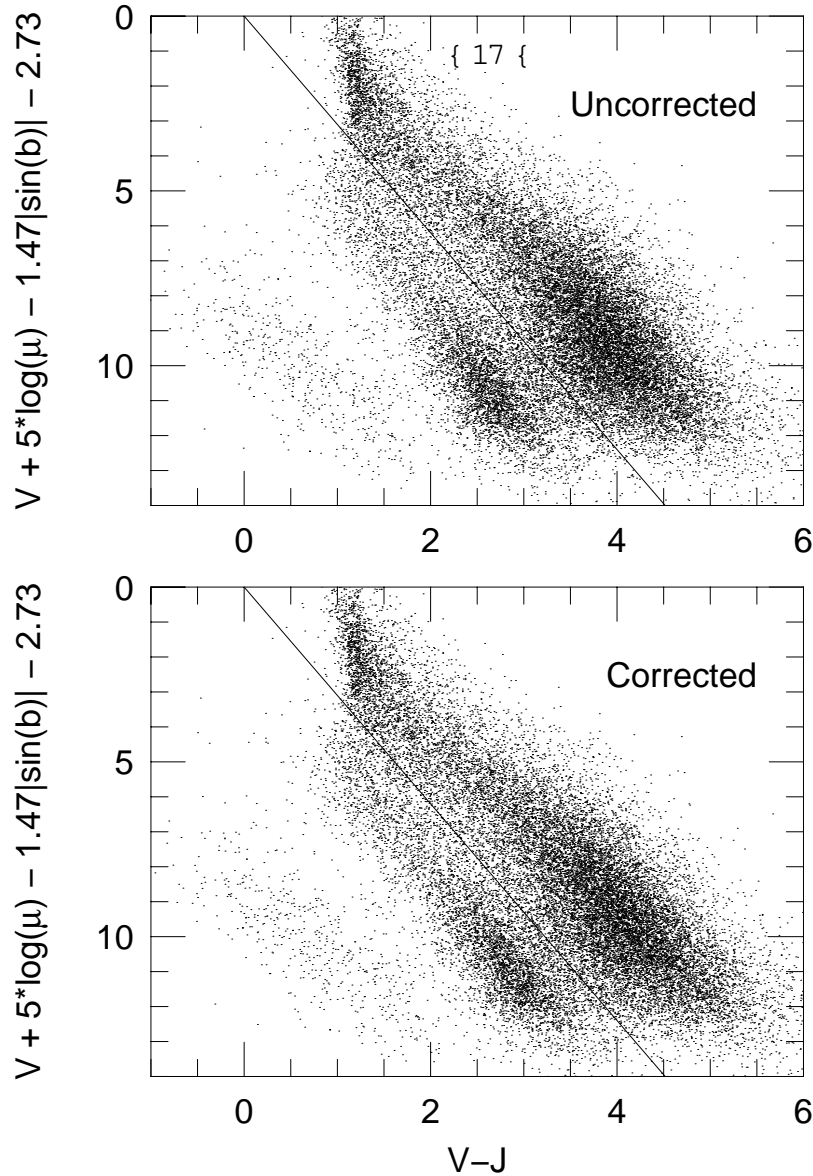


Fig. 2. | Reduced proper motion (RPM) diagram before (upper) and after (lower) calibration of NLTT V band photometry. Following Salim & Gould (2003), the RPM includes a term that depends on Galactic latitude ( $b$ ) as well as proper motion ( $\mu$ ),  $V_{\text{RPM,adj}} = V + 5 \log(\mu) - 1.47 |\sin(b)| - 2.73$ . This quantity enters the discriminant  $V_{\text{RPM,adj}} - 3.1(V - J)$ . Salim & Gould (2003) adopted  $V - J = 0$  (solid line) as a boundary between halo stars (below) and disk and thick-disk stars (above). The new calibration moves the faint end of both the halo and disk sequences toward the red and straightens and somewhat cleans up the "trough" between the halo and disk populations. We still regard  $V - J = 0$  as a good boundary between disk and halo stars.

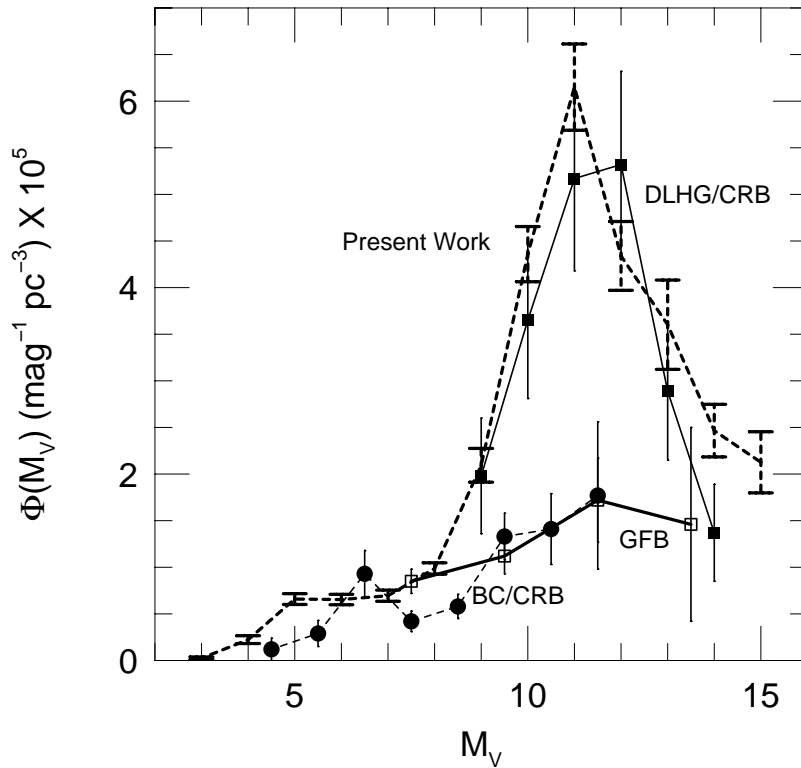


Fig. 3. Comparison of the halo luminosity function (LF) derived in the present work (bold dashed curve) using calibrated rNLT T photometry with several previous determinations. The rNLT T LF is now in good agreement with the parallax-based determination of Dahn et al. (1995) as renormalized by Gould (2003a) based on results from Casertano et al. (1990), which is shown as a solid curve (DLHG/CRB). These are both local measurements, so they should agree, but in an analysis prior to the new calibration (Gould 2003a, 2004), the rNLT T determination peaked about 1 mag brighter than DLHG/CRB. The measurement of Gould et al. (1997) (GFB) agrees with the present work at bright magnitudes but shows a much weaker peak. However, it is based on a distant sample, so in principle may be probing a different population. Also shown is the determination of Bahcall & Casertano (1986) as renormalized by Gould (2003a) using CRB (BC/CRB).

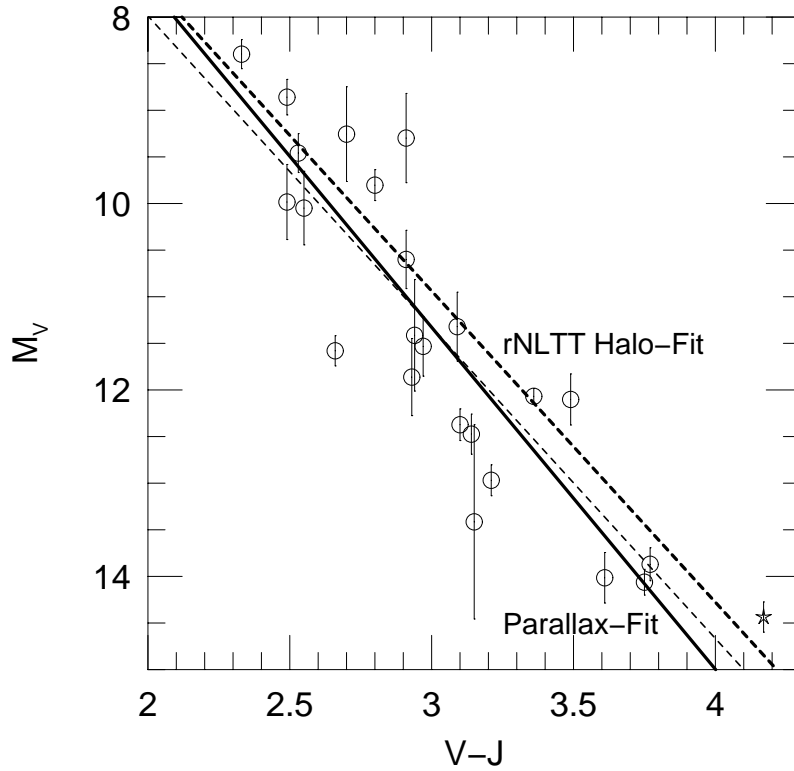


Fig. 4. Parallax-based absolute magnitudes  $M_V$  and  $(V - J)$  colors of 23 stars (circles) used to estimate the color-magnitude relation (CMR), given by eq. (10) and shown as a bold solid curve. Also shown is one star that is excluded from the fit (star). The error bars on the points reflect only the parallax errors and not the  $0.72 \text{ mag}$  "cosmic scatter" that was added in the fitting process. The bold dashed curve shows the CMR derived from the fit to rNLTT halo stars presented in this paper. When the parallax-fit is forced to have the same slope as the rNLTT halo model (which has much higher statistical weight), its track is given by the thin dashed curve. When the parallax data are combined with the rNLTT halo fit, the resulting CMR is parallel to and roughly halfway between the two dashed curves. Its form is given by eq. (12), but it is not shown in this figure to avoid clutter.

Table 1. Halo Parameters with Calibrated NLT T Photometry

Parameter	Units	Old Value	New Value	Old Error	New Error
$(M_v = 3)$	$10^5 \text{ pc}^3$	0:030	0:022	0:010	0:014
$(M_v = 4)$	$10^5 \text{ pc}^3$	0:170	0:244	0:030	0:042
$(M_v = 5)$	$10^5 \text{ pc}^3$	0:490	0:647	0:060	0:058
$(M_v = 6)$	$10^5 \text{ pc}^3$	0:610	0:654	0:060	0:056
$(M_v = 7)$	$10^5 \text{ pc}^3$	0:640	0:675	0:060	0:060
$(M_v = 8)$	$10^5 \text{ pc}^3$	0:860	0:987	0:090	0:061
$(M_v = 9)$	$10^5 \text{ pc}^3$	2:240	2:126	0:170	0:181
$(M_v = 10)$	$10^5 \text{ pc}^3$	4:660	4:314	0:420	0:296
$(M_v = 11)$	$10^5 \text{ pc}^3$	4:500	6:208	0:420	0:463
$(M_v = 12)$	$10^5 \text{ pc}^3$	2:570	4:190	0:320	0:369
$(M_v = 13)$	$10^5 \text{ pc}^3$	2:070	3:727	0:370	0:479
$(M_v = 14)$	$10^5 \text{ pc}^3$	1:660	2:376	0:330	0:282
$(M_v = 15)$	$10^5 \text{ pc}^3$	1:530	2:126	0:450	0:328
$U_1$	$\text{km s}^{-1}$	8:500	10:582	2:200	1:408
$U_3$	$\text{km s}^{-1}$	7:500	6:395	2:400	1:787
$C_{11}^{1=2}$	$\text{km s}^{-1}$	167:900	165:580	1:400	2:426
$C_{22}^{1=2}$	$\text{km s}^{-1}$	113:000	115:279	1:700	3:481
$C_{33}^{1=2}$	$\text{km s}^{-1}$	88:600	89:342	1:900	2:259
$e_{12}$		0:008	0:017	0:014	0:015
$e_{13}$		0:014	0:010	0:023	0:017
$e_{23}$		0:039	0:036	0:026	0:025
a		3:590	3:339	0:010	0:027
b		0:690	0:921	0:010	0:073
$f_{\text{break}}$		0:500	0:384	0:060	0:027
$V_{\text{break}}$		18:270	18:809	0:040	0:102
	$\text{kpc}^{-1}$	2:700	3:257	1:000	0:734
	$\text{kpc}^{-1}$	0:019	0:059	0:057	0:054

